

# **Bilayer ultrathin amorphous carbon films synthesized by filtered cathodic vacuum arc for magnetic storage technology**

J. Xie and K. Komvopoulos

Department of Mechanical Engineering, University of California, Berkeley, CA 94720, USA

## **Abstract**

Bilayer deposition of amorphous carbon (*a*-C) films was used to reduce the thickness of the interface layer and improve the film uniformity. Changes in the cross-sectional structure of hydrogen-free ultrathin *a*-C films deposited by filtered cathodic vacuum arc were studied by transmission electron microscopy and electron energy loss spectroscopy. It is shown that by depositing first an ultrathin (<1 nm) buffer layer under no substrate bias conditions and then switching to substrate biasing to deposit the *a*-C film, the thickness of the interface layer is decreased from 1.2 to 0.5 nm, while the thickness of the bulk layer is increased from 1.4 to 2.1 nm, resulting in a total film thickness of 3.8 nm. While this technique effectively reduces the *a*-C film thickness it does not affect the film's nanostructure (e.g.,  $sp^3$  content). The results of this study reveal the high potential of bilayer deposition to produce ultrathin *a*-C films with relatively high  $sp^3$  content for high-density magnetic recording.

## I. INTRODUCTION

The high hardness and excellent wear and corrosion resistance of amorphous carbon (*a*-C) films [1–3] make them prime overcoat materials for hard-disk drives (HDDs). The origin of the good tribomechanical properties of *a*-C films is the relatively high content of tetrahedral ( $sp^3$ ) atomic carbon hybridization, which controls the density, elasticity, and hardness. The  $sp^3$  content shows a strong dependence on the process conditions and deposition method. Energetic film deposition methods, such as filtered cathodic vacuum arc (FCVA) [4], which use ions as film-forming precursors, are particularly effective in producing ultrathin *a*-C films with high  $sp^3$  contents. This is because the  $C^+$  ion kinetic energy can be tuned by biasing the substrate holder with an optimum pulsed voltage to control direct and recoil ion implantation, sputtering of weakly bonded surface atoms (densification), and deposition. However, partial backscattering of the  $C^+$  ions and reduced ion bombardment on the surface of the growing film during the final stage of film deposition yield a multilayered film structure consisting of interface and surface layers of relatively low and varying  $sp^3$  contents and intermediate (bulk) layer rich in  $sp^3$  hybridization [5–10].

Current trends in magnetic recording necessitate the decrease of the physical spacing between the magnetic media and read/write transducer embedded into the flying head to  $\sim 5$  nm [11,12]. To achieve such a small physical spacing, the overcoat thickness must be reduced to  $\sim 2$ – $3$  nm. However, decreasing the film thickness to such extremely low levels raises a concern about its uniformity, density, and overall protective capacity because it will enhance the dominance of the  $\sim 1$ – $2$ -nm-thick interface and surface layers, which are rich in  $sp^2$  hybridization. Indeed, it has been reported that the tribomechanical properties (e.g., elastic modulus and wear rate) and  $sp^3$  content show a dependence on film thickness when the films are  $< 4$  nm thick [13–17]. Moreover, the important effect of  $sp^3$  content on the thermal stability of *a*-C films used in heat-assisted magnetic recording (HAMR) has been elucidated by molecular dynamic simulation results [18]. Thus, it is necessary to develop a film deposition method, which can produce

ultrathin *a*-C films with structures and properties predominantly controlled by the  $sp^3$ -rich bulk layer and interface and surface layers of minimal thickness.

Previous studies dealing with the adhesion of *a*-C films to different substrate materials examined relatively thick films. The increase of the substrate bias voltage promotes intermixing of carbon with the substrate atoms, which is conducive to the development of a strong film/substrate interface [19–22]. However, this will also increase the thickness of the interface layer, which may negatively impact the magnetics of the media [4,13] and degrade the quality of the ultrathin film as a result of the intense  $C^+$  ion bombardment [13,23].

The main objective of this study is to introduce a multi-step FCVA deposition process which can overcome the aforementioned problems. The main concept is to synthesize bilayer ultrathin *a*-C films with structure and properties dominated by the  $sp^3$ -rich bulk layer. An initial low ion energy deposition step (no substrate biasing) and a final process step of  $Ar^+$  ion sputter etching are used before and after *a*-C film deposition under optimum FCVA conditions of substrate biasing, respectively. The initial deposition step leads to the formation of an extremely thin buffer layer that acts as a buffer layer in the subsequent process step of bulk layer deposition under energetic  $C^+$  ion bombardment (substrate biasing). Therefore, another principal objective is to examine the through-thickness structure and composition of bilayer ultrathin (~2–3 nm) *a*-C films deposited by this method using high-resolution transmission electron microscopy (HRTEM) and electron energy loss spectroscopy (EELS). To illustrate the capability of the present multi-step FCVA process to synthesize ultrathin *a*-C films mainly consisting of  $sp^3$ -rich bulk layer, representative HRTEM and EELS results of bilayer *a*-C films are contrasted with those of single-layer *a*-C films deposited under the same FCVA conditions as the bulk layer of the bilayer films.

## II. EXPERIMENTAL PROCEDURES

### A. Film Synthesis

Substrates ( $1 \times 1 \text{ cm}^2$ ) cut from a 2.5-in.-diameter disk coated with a  $\sim 100$ -nm-thick NiTa layer were loaded onto a custom-made FCVA system [24,25] and etched for 6 min in vacuum ( $\sim 2 \times 10^{-4}$  Torr) with a 500-eV  $\text{Ar}^+$  ion beam of  $60^\circ$  incidence angle (measured from the normal to the substrate surface) generated by a 64-mm Kaufman ion source (Commonwealth Scientific, Alexandria, VA). After allowing the substrate to cool for 5 min and the chamber vacuum to reach a low base pressure ( $< 5 \times 10^{-7}$  Torr), plasma arcing was initiated at the cathode (99.99% pure graphite) surface with a mechanical striker. The plasma was stabilized by applying to the cathode a cusp-configuration magnetic field [24]. The potential and current between the graphite cathode and the anode were set at  $\sim 24$  V and  $\sim 89$  A, respectively. The magnetic field generated by electromagnetic coils having an out-of-plane S configuration was used to filter out any macroparticles and/or droplets ejected from the cathode surface and ensure that only high-purity ( $\sim 99.99\%$ )  $\text{C}^+$  ions exit from the filter. The current of the auxiliary, upstream, and downstream coils was set at 30.5, 30.9, 29.6 A, respectively. For uniform sputter etching and film growth in the radial direction, the substrate was rotated at 60 rpm during both  $\text{Ar}^+$  ion bombardment and film deposition processes.

To control the  $\text{C}^+$  ion energy during the first deposition step and minimize the thickness of the buffer layer, the substrate stage was oriented at an angle of  $20^\circ$  with respect to incoming  $\text{C}^+$  ions without applying a bias voltage. To produce a buffer layer of thickness  $< 1$  nm, the deposition time was fixed at 6 s. During the second step of deposition, which also lasted for 6 s, an optimal pulsed bias voltage of  $-100$  V and 75% duty cycle was applied to the substrate stage which was placed perpendicular to the incoming  $\text{C}^+$  ions to favor ion subplantation into the buffer layer and promote  $sp^3$  hybridization in the bulk layer [26]. In the third deposition step, 500-eV  $\text{Ar}^+$  ion sputter etching was performed for 6 min to reduce the film thickness to 2–3 nm, as demonstrated in a previous study [27]. The process conditions of each

deposition step are summarized in Table 1. For comparison, a single-layer *a*-C film was deposited in 12 s under optimal FCVA conditions (i.e., substrate bias voltage = -100 V, duty cycle = 75%, ion incidence angle = 90°) and etched to a similar thickness as the bilayer films by a 4-min Ar<sup>+</sup> ion sputter etching.

## B. Microanalysis Methods

Cross-sectional HRTEM samples were prepared by mechanical grinding, two-side dimpling, and surface finishing by ion milling. Before sample bonding, a thin (5–10 nm) Au capping layer was sputtered onto the surface to facilitate the distinction of the epoxy glue from the *a*-C film in HRTEM and to separate the carbon film EELS signal from the carbon-based epoxy glue. More details about the HRTEM sample preparation method used in this study can be found elsewhere [26,28,29].

A FEI Tecnai (F20 UT) microscope operated at 200 kV, equipped with a CCD camera (2048 × 2048 pixels) positioned 42 mm behind the Gatan imaging filter, was used to obtain the HRTEM images and EELS spectra. The EELS collection semi-angle was set at 16.3 mrad. A 150- $\mu$ m C2 aperture and a 9.4-mrad C2 semi-angle were used in this study. The spatial resolution of the scanning TEM (STEM) (without a monochromator) is equal to 0.14 nm. Using the full-width at half-maximum of the zero-loss peak, the energy resolution of the EELS was found to be  $\leq 0.58$  eV, which considering the band gap difference (0.8–0.9 eV) between  $sp^2$  and  $sp^3$ , is sufficient for distinguishing  $sp^2$  and  $sp^3$  hybridizations.

## III. RESULTS AND DISCUSSION

Cross-sectional HRTEM specimens were used to determine the *a*-C film thickness after each process step. Fig. 1 shows cross-sectional HRTEM images of *a*-C films obtained after each step. (The different layers within the cross-sectional structure are labeled in Fig. 1(c)). All images reveal a multi-layer structure consisting of (1) NiTa layer, (2) *a*-C film, (3) Au capping layer, and (4) epoxy glue. The average film thickness corresponding to the first, second, and third process step is equal to 0.96, 5.89, and 2.50 nm, respectively (Table 1).

The cross-sectional elemental structure of the *a*-C films was examined by the analytical EELS, which uses the energy loss of electrons passing through the specimen due to inelastic collisions of incoming incident electrons with electrons in the specimen atoms [30,31]. The high-energy-loss range (>50 eV) of the EELS spectrum provides insight into beam electron interaction with inner (core-shell) electrons of the specimen material. The characteristic K-edge spectrum of carbon is in the range of 280–305 eV, and can be used to determine the  $sp^2$  and  $sp^3$  contents of the *a*-C film. The pre-edge peak at 285 eV is attributed to electron excitation from the ground-state 1s core level to the vacant  $\pi^*$ -like anti-bonding states, whereas the edge starting from 290 eV is due to electron excitation from 1s core level to the  $\sigma^*$  states [32]. The elemental composition can be obtained from an analysis of the K-edge spectra. The  $\sigma^*$  peak is integrated within the energy window from 290 to 305 eV, to minimize plural scattering effects, while the  $\pi^*$  peak is fitted with a Gaussian distribution. The area ratio of these two peaks is proportional to the relative number of  $\sigma^*$  and  $\pi^*$  orbitals, which is 3/1 for 100%  $sp^2$  and 4/0 for 100%  $sp^3$ . Therefore, the content  $x$  of  $sp^2$ -bonded carbon atoms in the film is given by [32]

$$\frac{(\pi^*/\sigma^*)_{\text{film}}}{(\pi^*/\sigma^*)_{\text{std}}} = \frac{3x}{4-x} \quad (1)$$

where the standard (std) sample consists of 100%  $sp^2$  evaporated carbon film. More details about curve fitting and calculation of the  $sp^3$  fraction are given elsewhere [5,26].

Fig. 2 shows the cross-sectional structure of *a*-C films after each process step. The normalized carbon intensity is obtained by integrating the EELS spectrum from 280 to 305 eV and then dividing the result with the peak intensity obtained across the depth profile. The  $sp^3$  fraction is calculated from C K-edge spectra using Eq. (1). The carbon concentration and  $sp^3$  fraction depth profiles reveal the existence of five distinct layers with the following characteristics: (i) *substrate* (the carbon signal intensity is almost zero because the signal corresponds to the NiTa layer); (ii) *interface (buffer) layer* (the carbon concentration and  $sp^3$  content increases sharply); (iii) *bulk layer* (the carbon concentration stabilizes at

~100% while the  $sp^3$  fraction remains almost constant); (iv) *surface layer* (both the carbon concentration and the  $sp^3$  fraction decrease sharply); and (v) *capping layer* (the weak carbon signal intensity is attributed to physisorption of adventitious carbon to the surface of the Au layer surface). The dashed lines shown in Fig. 2 denote the boundaries of neighboring layers. A comparison of the results shown in Fig. 2 indicates that the bilayer film structure exhibits a sharp increase in  $sp^3$  content in the buffer (interface) layer and that  $Ar^+$  ion sputter etching effectively reduced the thickness of the surface layer, consistent with previous findings [27].

Fig. 3 shows a comparison of cross-sectional HRTEM images for a single-layer and bilayer *a*-C films of similar thickness. The corresponding depth profiles of the normalized carbon intensity and  $sp^3$  content, obtained from cross-sectional scanning of the EELS spectra, are contrasted in Fig. 4. It can be seen that the thickness of interface layer is significantly reduced and the change (slope) of the  $sp^3$  content in the interface layer is much larger in the bilayer *a*-C film.

The thickness of the interface (buffer), bulk, and surface layers and the average  $sp^3$  content of the bulk layer of single-layer and bilayer *a*-C films are given in Table 2. The sum of the thicknesses of all layers is termed total thickness. The HRTEM and EELS results of the total thickness are in good agreement. The difference of the total thickness measured from the HRTEM and EELS results indicates some intermixing of carbon with the NiTa layer, which is not captured in the HRTEM images. Therefore, the carbon signal detected by EELS provides a more accurate measurement of the total thickness. Table 2 shows that the surface and total thickness of the single-layer and bilayer *a*-C films are similar; however, the interface layer in the bilayer films has a much smaller thickness. The similar thickness of the surface layer is expected because both single-layer and bilayer *a*-C films were subjected to the same  $Ar^+$  ion sputter etching post-deposition treatment. Thus, the interface layer thickness decreases from 31.6% (single-layer film) to 13.1% (bilayer film) of the total film thickness, while the bulk layer thickness increases from 36.8% (single-layer film) to 55.3% (bilayer film) of the total film thickness. In addition, the slope of the

$sp^3$  depth profile in the interface layer changes from 31.4%/nm (single-layer film) to 60%/nm (bilayer film) and the  $sp^3$  content of the bulk layer increases from 51.9% (Single-layer film) to 53% (bilayer film). These results demonstrate the high potential of bilayer  $a$ -C film deposition by FCVA.

#### IV. CONCLUSIONS

The thickness, structure, and composition of single- and bilayer  $a$ -C films synthesized by FCVA were characterized by cross-sectional HRTEM and EELS. Depositing first an ultrathin (~1 nm) buffer layer under zero substrate bias voltage, the thickness of the interface (intermixing) layer was reduced by 58%, which is critical to preserving the properties of magnetic media. In addition, the  $sp^3$  fraction in the bulk layer of the bilayer  $a$ -C films was slightly increased. The obtained HRTEM and EELS results indicate that the bilayer film deposition technique developed in this study can effectively reduce the overcoat thickness in magnetic recording, while preserving the overcoat quality and enhancing cross-sectional film uniformity.

#### ACKNOWLEDGMENTS

This research was funded by the Computer Mechanics Laboratory, University of California, Berkeley. The TEM/EELS studies were carried out at the National Center for Electron Microscopy, Molecular Foundry, Lawrence Berkeley National Laboratory (Proposal No. 1886). Work at the Molecular Foundry is supported by the Office of Science, Office of Basic Energy Sciences, U.S. Department of Energy (Contract No. DE-AC02-05CH11231).

#### REFERENCES

- [1] A. Grill, *Diam. Relat. Mater.* **8**, 428, 1999.
- [2] J. Robertson, *Diamond-like amorphous carbon*, *Mater. Sci. Eng. R: Reports* **37**, 129–281, 2002.

- [3] H.-S. Zhang and K. Komvopoulos, Surface modification of magnetic recording media by filtered cathodic vacuum arc, *J. Appl. Phys.* **106**, 093504, 2009.
- [4] I. G. Brown, Cathodic arc deposition of films, *Annu. Rev. Mater. Sci.* **28**, 243–269, 1998.
- [5] N. Wang and K. Komvopoulos, *J. Mater. Res.* **28**, 2124, 2013.
- [6] M. P. Siegal, P. N. Provencio, D. R. Tallant, R. L. Simpson, B. Kleinsorge, and W. I. Milne, *Appl. Phys. Lett.* **76**, 2047, 2000.
- [7] C. A. Davis, G. A. J. Amaratunga, and K. M. Knowles, *Phys. Rev. Lett.* **80**, 3280, 1998.
- [8] C. A. Davis, K. M. Knowles, and G. A. J. Amaratunga, *Surf. Coat. Technol.* **76/77**, 316, 1995.
- [9] E. Riedo, F. Comin, J. Chevrier, F. Schmithusen, S. Decossas, and M. Sancrotti, *Surf. Coat. Technol.* **125**, 124, 2000.
- [10] Y. Lifshitz, S. R. Kasi, J. W. Rabalais, and W. Eckstein, *Phys. Rev. B* **41**, 10468, 1990.
- [11] J. Robertson, Requirements of ultrathin carbon coatings for magnetic storage technology, *Tribol. Int.* **36**, 405–415, 2003.
- [12] P. R. Goglia, J. Berkowitz, J. Hoehn, A. Xidis, and L. Stover, Diamond-like carbon applications in high density hard disc recording heads, *Diam. Relat. Mater.* **10**, 271–277, 2001.
- [13] A. C. Ferrari, Diamond-like carbon for magnetic storage disks, *Surf. Coat. Technol.* **180/181**, 190–206, 2004.
- [14] C. Casiraghi, A. C. Ferrari, J. Robertson, R. Ohr, M. v. Gradowski, D. Schneider, and H. Hilgers, Ultra-thin carbon layer for high density magnetic storage devices,” *Diam. Relat. Mater.* **13**, 1480–1485, 2004.
- [15] C. Casiraghi, A. C. Ferrari, R. Ohr, D. Chu, and J. Robertson, Surface properties of ultra-thin tetrahedral amorphous carbon films for magnetic storage technology, *Diam. Relat. Mater.* **13**, 1416–1421, 2004.

- [16] M. G. Beghi, A. C. Ferrari, K. B. K. Teo, J. Robertson, C. E. Bottani, A. Libassi, and B. K. Tanner, Bonding and mechanical properties of ultrathin diamond-like carbon films, *Appl. Phys. Lett.* **81**, 3804–3806, 2002.
- [17] M. Zhong, C. Zhang, J. Luo, and X. Lu, The protective properties of ultra-thin diamond like carbon films for high density magnetic storage devices, *Appl. Surf. Sci.* **256**, 322–328, 2009.
- [18] B. Marchon, et al., Head–disk interface materials issues in heat-assisted magnetic recording, *IEEE Trans. Magn.* **50**, 137-143, 2014.
- [19] D. Sheeja, et al., Tribological properties and adhesive strength of DLC coatings prepared under different substrate bias voltages, *Wear* **249**, 433–439, 2001.
- [20] C. A. Davis, G. A. J. Amaratunga, and K. M. Knowles, *Phys. Rev. Lett.* **80**, 3280, 1998.
- [21] M. Chhowalla and G. A. J. Amaratunga, Strongly adhering and thick highly tetrahedral amorphous carbon (ta-C) thin films via surface modification by implantation, *J. Mater. Res.* **16**, 5-8, 2001.
- [22] E. Rismani, et al., Effect of pretreatment of Si interlayer by energetic C<sup>+</sup> ions on the improved nanotribological properties of magnetic head overcoat, *J. Appl. Phys.* **111**, 084902, 2012.
- [23] H. Han, F. Ryan, and M. McClure, Ultra-thin tetrahedral amorphous carbon film as slider overcoat for high areal density magnetic recording, *Surf. Coat. Technol.* **120**, 579-584, 1999.
- [24] H.-S. Zhang and K. Komvopoulos, Direct-current cathodic vacuum arc system with magnetic-field mechanism for plasma stabilization, *Rev. Sci. Instrum.* **79**, 073905(1-7), 2008.
- [25] H.-S. Zhang and K. Komvopoulos, Synthesis of ultrathin carbon films by direct current filtered cathodic vacuum arc, *J. Appl. Phys.* **105**, 083305(1-7), 2009.
- [26] J. Xie and K. Komvopoulos, The role of duty cycle of substrate pulse biasing in filtered cathodic vacuum arc deposition of amorphous carbon films, *IEEE Trans. Magn.* **51**, 3302009(1-9), 2015.
- [27] J. Xie and K. Komvopoulos, The effect of Argon ion beam irradiation on the thickness and structure of ultrathin amorphous carbon films, *J. Appl. Phys.*, 2015 (submitted).

- [28] D. Wan and K. Komvopoulos, Transmission electron microscopy and electron energy loss spectroscopy analysis of ultrathin amorphous carbon films, *J. Mater. Res.* **19**, 2131–2136, 2004.
- [29] N. Wang and K. Komvopoulos, Incidence angle effect of energetic carbon ions on deposition rate, topography, and structure of ultrathin amorphous carbon films deposited by filtered cathodic vacuum arc, *IEEE Trans. Magn.* **48**, pp. 2220–2227, 2012.
- [30] D. B. Williams and C. B. Carter, *Transmission Electron Microscopy: A Textbook for Materials Science* (Springer, New York, 2009), Ch. 37, pp. 679–681.
- [31] R. F. Egerton, *Electron Energy-Loss Spectroscopy in the Electron Microscope* (3<sup>rd</sup> ed., Springer, New York, 2011), Ch. 3, pp. 111–229.
- [32] J. J. Cuomo, J. P. Doyle, J. Bruley, and J. C. Liu, Sputter deposition of dense diamond-like carbon films at low temperature, *Appl. Phys. Lett.* **58**, 466–468, 1991.

Table 1. Deposition conditions of bilayer *a*-C films.

Process step	Process conditions				Characteristics	Film thickness (nm)
	Duty cycle (%)	Substrate bias voltage (V)	Ar <sup>+</sup> ion incidence angle (°)	Time (s)		
1	–	0	20	6	thin buffer layer	0.96
2	75	–100	90	6	high <i>sp</i> <sup>3</sup> bulk layer	5.89
3	Ar <sup>+</sup> ion etch: 500 eV, 6 min, 30°, 2 × 10 <sup>–4</sup> Torr				etched to ~2 nm	2.50

Table 2. Total thickness, surface, bulk, and interface (buffer) layer thickness, and average  $sp^3$  content of bulk layer of single-layer and bilayer  $a$ -C films synthesized by FCVA.

Properties	bilayer	single-layer
Total thickness from TEM (nm)	2.5	2.3
Total thickness from EELS (nm)	3.7	3.7
Surface layer thickness from EELS (nm)	1.2	1.2
Bulk layer thickness from EELS (nm)	2.1	1.2
Bulk layer-to-total thickness percentage ratio (%)	56.8	32.4
Interface layer thickness from EELS (nm)	0.4	1.3
Interface layer-to-total thickness percentage ratio (%)	10.8	35.1
Change in slope of $sp^3$ profile in the interface layer (%/nm)	60.0	31.4
Average $sp^3$ content of bulk layer (at%)	$53.0 \pm 3.6$	$51.9 \pm 1.4$

## List of Figures

- Fig. 1. Cross-sectional HRTEM images of *a*-C films deposited by FCVA after the deposition of (a) a buffer (interface) layer and (b) a bulk layer and (c) after 6-min of Ar<sup>+</sup> ion etching post-deposition treatment. Contrast and structure differences reveal (1) NiTa layer, (2) *a*-C film, (3) Au capping layer, and (4) epoxy mounting material.
- Fig. 2. Depth profiles of normalized carbon intensity of C-K edge and *sp*<sup>3</sup> content calculated from the C K-edge spectra of *a*-C films deposited by FCVA after deposition of a buffer (interface) layer and a bulk layer, and after 6-min of Ar<sup>+</sup> ion etching post-deposition treatment. The dashed lines indicate the boundaries between neighboring regions.
- Fig. 3. Cross-sectional HRTEM images of (a) single-layer and (b) bilayer *a*-C films deposited by FCVA obtained after 6-min of Ar<sup>+</sup> ion etching post-deposition treatment.
- Fig. 4. Depth profiles of normalized carbon intensity of C-K edge and *sp*<sup>3</sup> content calculated from the C K-edge spectra of *a*-C films deposited by FCVA. The depth profiles reveal significant differences between single-layer and bilayer *a*-C films after 6-min of Ar<sup>+</sup> ion etching post-deposition treatment. The dashed lines indicate the boundaries between neighboring regions.

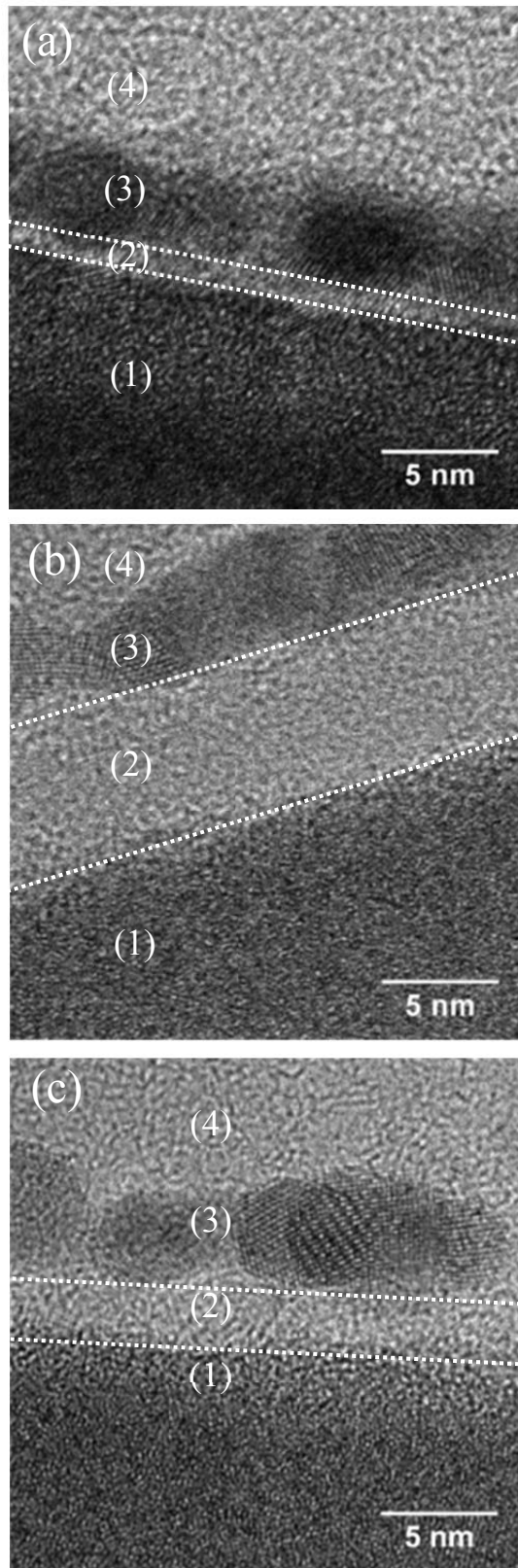


Fig. 1. Cross-sectional HRTEM images of *a*-C films deposited by FCVA after the deposition of (a) a buffer (interface) layer and (b) a bulk layer and (c) after 6-min of  $\text{Ar}^+$  ion etching post-deposition treatment. Contrast and structure differences reveal (1) NiTa layer, (2) *a*-C film, (3) Au capping layer, and (4) epoxy mounting material.

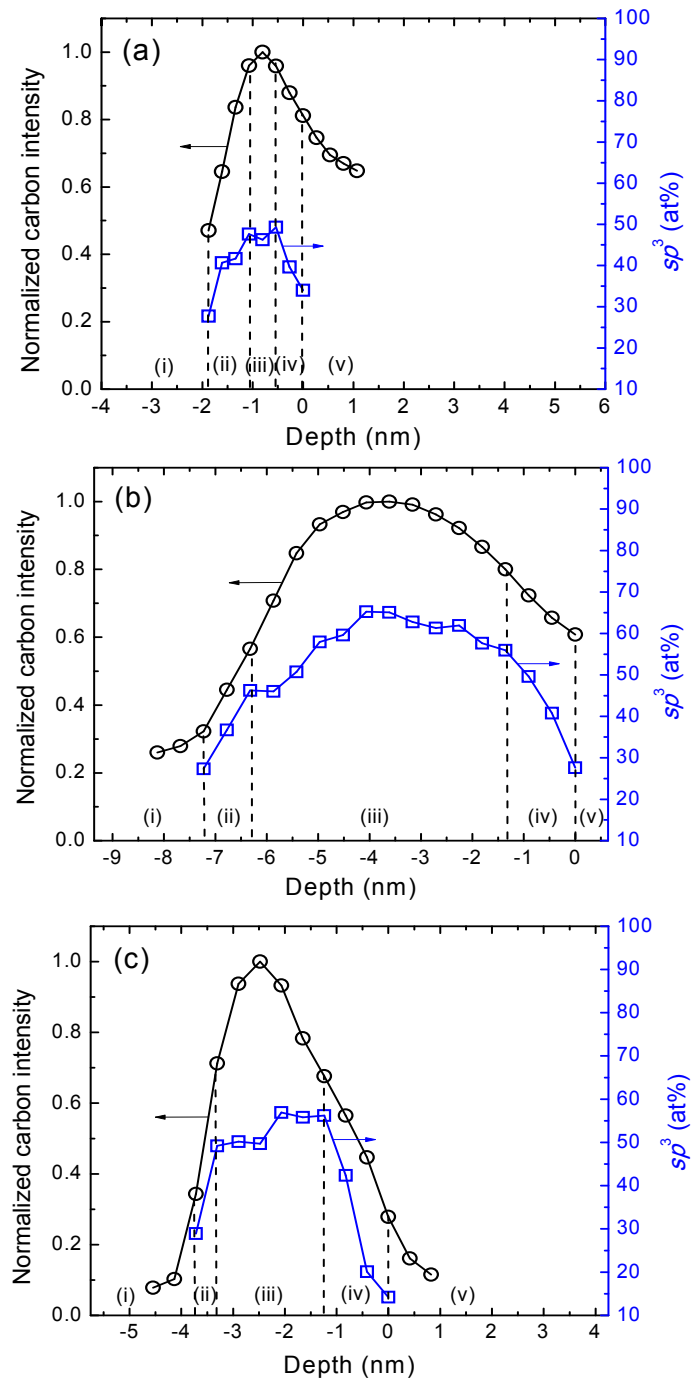


Fig. 2. Depth profiles of normalized carbon intensity of C-K edge and  $sp^3$  content calculated from the C K-edge spectra of  $a$ -C films deposited by FCVA after deposition of a buffer (interface) layer and a bulk layer, and after 6-min of  $Ar^+$  ion etching post-deposition treatment. The dashed lines indicate the boundaries between neighboring regions.

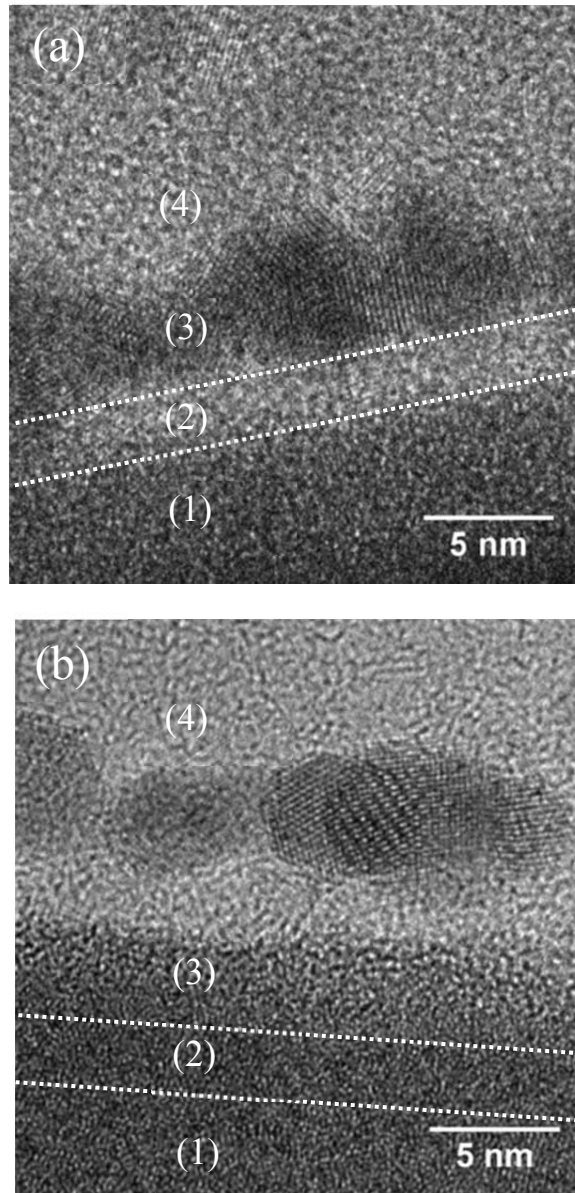


Fig. 3. Cross-sectional HRTEM images of (a) single-layer and (b) bilayer *a*-C films deposited by FCVA obtained after 6-min of Ar<sup>+</sup> ion etching post-deposition treatment.

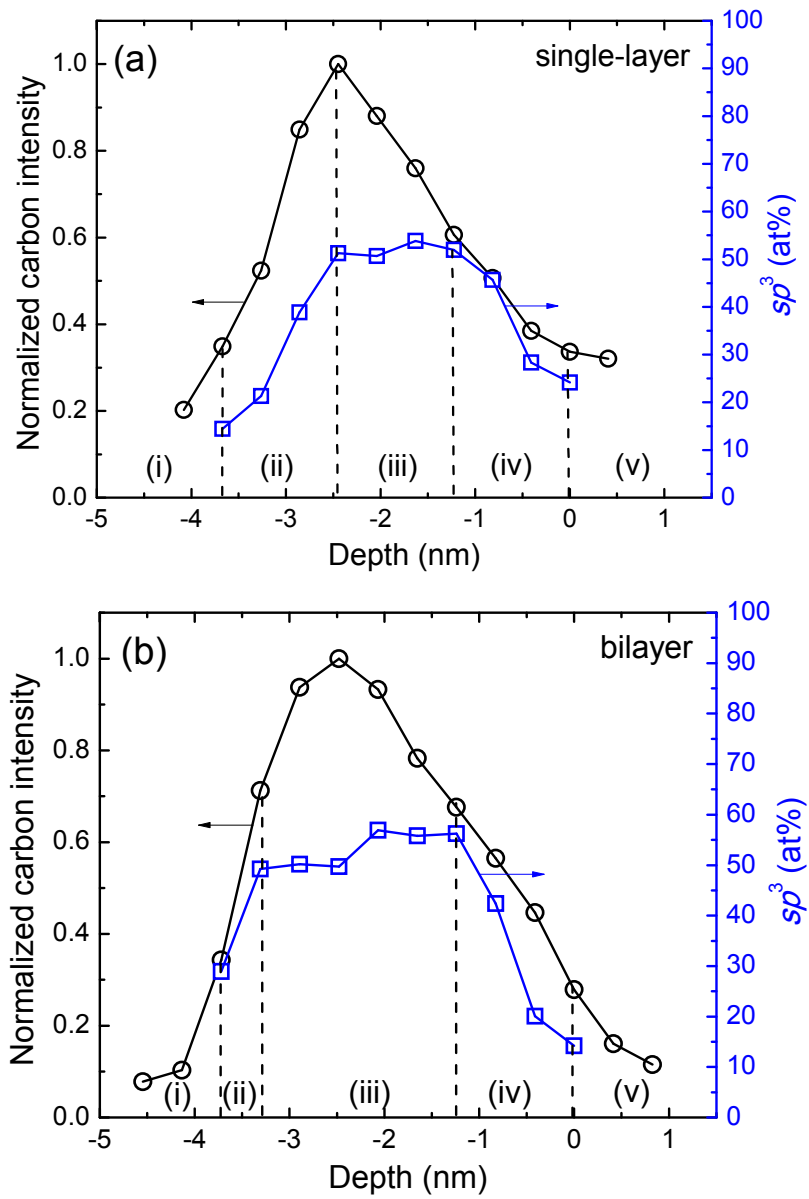


Fig. 4. Depth profiles of normalized carbon intensity of C-K edge and  $sp^3$  content calculated from the C K-edge spectra of *a*-C films deposited by FCVA. The depth profiles reveal significant differences between single-layer and bilayer *a*-C films after 6-min of  $Ar^+$  ion etching post-deposition treatment. The dashed lines indicate the boundaries between neighboring regions.